Influence of n-Mosfet transistor on dye-sensitized solar cell efficiency

Temitope Abodunrin [a],*, Adenike Boyo [b], Mojisola Usikalu [a], Moses Emetere [a], Oluseyi Ajayi [c], Chester Kotsedi [d], Zebib Nuru [d], Maaza Malik [d], Godwin Oghonyon [e]

[a] *Department of Physics, Covenant University, Nigeria*

[b] *Department of Physics, Lagos State University, Nigeria*

[c] *Department of Mechanical Engineering, Covenant University, Nigeria*

[d] *iThemba Labs, Western Cape, South Africa*

[e] *Department of Mathematics, Covenant University, Nigeria*

* Corresponding author.

E-mail address: Temitope.Abodunrin@covenantuniversity.edu.ng (T. Abodunrin).

Abstract

A new strategy for evaluating the efficiency of Dye-sensitized Solar Cell (DSC) employed in this study was to introduce a device stabilizer which also functioned as an external load. This aim was accomplished through computations of efficiency of different DSCs based on n-Mosfet transistor. Transistor Z44 mosfet's impact on the DSC systems was to significantly moderate the effect of two vital components namel; the photoanodes and electrolyte sensitizers. The outcome of the Z44 mosfet incorporation inside the DSC was a synchronization in photovoltaic spectral responses thereby, minimizing the common limitations of DSCs such as dye synergy, redox kinematics, photophysics and roughness factor which is not restrictive to N719 dyes. This study presents the results of indium-doped tin oxide (ITO) conducting glass doped DSCs with different electrolytes enhanced with a transistor mosfet; short-circuit current density (I_{sc}) of 0.104 A cm^{-2}, open-circuit voltage (V_{oc}) of 240.6 mV, efficiency of 0.9 % and a fill factor of 0.12 obtained under 1 atmospheric air mass conditions. The implication of this result is possible reproducibility and modelling of *T. daniellii* Mosfet DSC based on the comparative analysis of the output performance of *T. daniellii*

DSC on TiO$_2$ and ZnO photoanode. This also gives impetus for further scientific inquiry.

Keywords: Energy, Materials science, Natural product chemistry, Organic chemistry

1. Introduction

A third facet of nanotechnology is gradually evolving through the capacity of specially fabricated nanoparticles to selectively convert incident light into other spectral regions [1]. In nano terms, these atoms have a fewer number of molecules as neighbors. This in effect causes several incomplete bonds as the portion of atoms at the surface increases. Consequently, these dangling bonds equally display their own unique binding properties different from that of the bulk property [2]. This condition arouses a scientific prospect of combining alloys with these hanging bonds with a view of introducing significant advantages [3]. However, such an integration could mitigate or generate strains intrinsically in Group IV semiconductors that would be used as they aggregate to develop direct band gaps [4]. Previous studies have shown that there are two salient features which has made these semiconductor materials gain such prominence in DSC technology [5]. The first factor is the characteristic strain they exhibit, it serves an important major role in electronics and photonics. Through the advent of tensile and compressive strains, electron mobility is influenced to increase or decrease directly [6]. Secondly, charge mobility is the other factor increased by strain, it has been used in different experiments to improve the performance of Si-based and GeSn-based MOSFETs [7]. This defines the motivation for this study, the innate ability of n-Mosfet (Z44) to spontaneously adapt to any cell irrespective of the current output of the load. This performance was tested on several dye-sensitized solar cells. They were designed to yield a maximum power output by connecting the DSC to the base of the n-Mosfet transistor as shown in Fig. 1.

Despite this amazing observation, mass production of dye-sensitized solar cells (DSCs) is still limited due to its reduced long-term stability and efficiency [8]. The problem of dye-desorption from the photoanode surface is a natural but persistent limitation of DSCs that occurs throughout the lifetime of the device. However, it is encouraging to note that, desorption of dye from the photoanode surface could be suppressed by controlling thermodynamic equilibrium [9]. In this wise, introduction of a Z44 Mosfet-transistor optimized light collection in *T. daniellii* dye-sensitized solar cells [10]. Improved device stabilities were recorded from n-DSCs of *T. daniellii* which encouraged further synthesis and characterization [11]. A contributor to this good result is alluded to the addition of several redox mediator electrolytes which instigated good interboundary relationship at the dye/photoanode interface [12]. There was a significant enhancement in ionic conductivity of both sets of
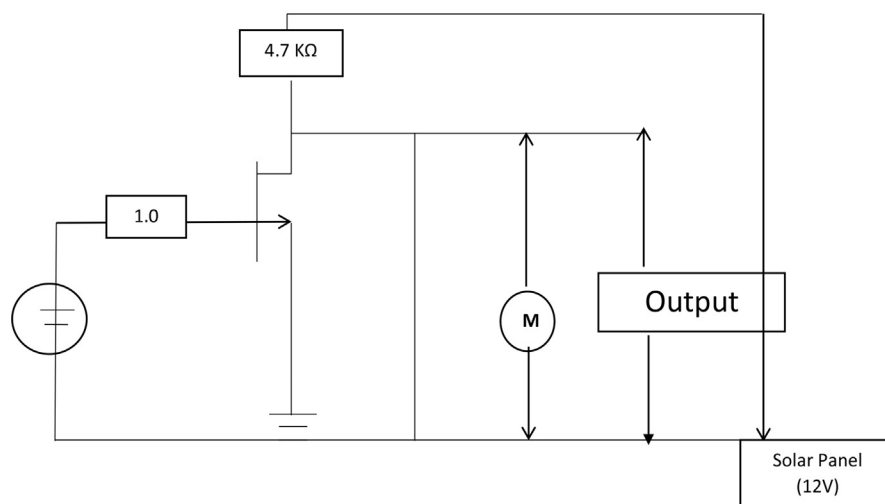
Fig. 1. n-Mosfet *T. daniellii* DSC.

mosfet transistor -based DSCs studied in this work. This improvement in ionic conductivity in turn produced a constant I-V trend which is absent in regular DSCs [13]. The implication of this result is that, the incorporation of a Z44 transistor produced a desired increase in conductivity of *T. daniellii* DSC by serving as part of the framework of the composite film. The underlying I^-/Cl^- ions also gave background electrocatalytic capacity which ultimately improved the operational electrocatalytic sites in the composite film.

Also noteworthy is the principal element for the determination of efficiency output of dye-sensitized solar cells (DSCs), the kinematics at the photoanode. Records give accounts of numerous substances which have been employed for use as photoanode material. This comprises heterogeneous materials such as Fe_2O_3, ZnO, p-Si, Cu_2O, GaN, GaP, $GaInP_2$ and $CuGaSe_2$, all of which have promising photochemical properties [14]. Many of these photoanode choices possess comparatively low band gaps which may be responsible for the general low efficiency output recorded in previous studies on these devices [15]. A desire to bridge this research gap led into an inquiry into other heterogeneous compounds such as GaAs, MoS_2, WSe_2 and $MoSe_2$ [16]. All these materials were also explored for their chemical stability but with minimal results. Further search for suitable photoanode materials with high efficiency boost ultimately led to the use of $SrTiO_3$ and $BaTiO_2$ and a discovery of their photocatalysis potential. A comparative study of the diverse results obtained from these diverse photoanodes brought about this hypothesis; TiO_2 and WO_3 were identified as the most prominent photoanode oxide materials for efficiency boost. A dual purpose for these photoanodes was a discovery of their suitability for oxidation of water, in addition to their aforementioned property as photoanode material [17]. Results have proven that, graphene-based materials also record excellent conductivity. Consequent on these findings is a limitation that, graphene is not as readily available

as TiO_2 and is more expensive. More comprehensive study in recent times revealed silicon based on 2 nm Nickel incorporated with steel as photoanode material; the observation was that even after 80 hours, there was no corrosion [18]. Despite all these myriad efforts, TiO_2 remains the most popular photoanode because of its low cost, availability and bio-compatibility with several organic compounds [19]. It is therefore imperative to discuss certain properties peculiar to TiO_2 which may be responsible for its remarkable photoelectrical properties.

Microscopic study reveals generally that, Anatase TiO_2 photoanode has a band gap of approximately 3.2 eV and width diameter of 10.1 mm at a range of 200 μm. In consonance with this finding, *T. daniellii* dye revealed its peak absorbance; λ_{max} at 0.767 a.u for a range of 390 nm wavelength in the visible range. In the near UV region, it showed λ_{max} of 232 nm and recorded its highest absorbance of 1.429 a.u. This was calculated and corresponds to photon energy of 1.3 eV. This implies that in practice, within an excitation span of a few nanoseconds, this amount of energy is used for ejecting an electron into the conduction band (CB) of the photoanode. Thus, the redox forward reaction shown as Eq. (1) illustrates ejection of iodide (I^-) which is about 0.6 times faster because it requires less energy than the back reaction which has an injection rate of 0.4. This further implies that; the driving force is stronger for I^- discharge than I^{3-}. This condition although largely responsible for slow injection rate, accounts for high efficiency in separation of charges. The resultant effect is that; trap sites accrue toward the conduction band edge of the photoanode. This build-up of charges creates a field, generating a barrier for even the particle size. This effectively renders the photoanode relatively impenetrable to the extent of restricting the transport mechanism to diffusion [20]. The characteristic period of wait, τ for an electron in a trap site before the next hop (provided density of trap site is sufficiently high enough) to a nearby site is explained by Fick's diffusion law. The most important reactions are illustrated by Eqs. (1), (2), and (3).

$$I_3^- + 2e^- + Pt \rightarrow 3I^- \tag{1}$$

$$\tau_{e^-} = I_3^- + 2e^- + 3I^- \tag{2}$$

$$D_L = D_{eff} * \tau_{e^-} \tag{3}$$

Where D_L is the diffusion length in cm, D_{eff} is the effective coefficient of diffusion in cms^{-1} and τ_{e-} is the lifetime of the electron in s. Thus, charge transport which is primarily due to electron hopping or diffusion is given from Fick's diffusion law as given by Eq. (4);

$$n * t * A = -D_{eff} * c \tag{4}$$

Where n is the number of electrons, A is the surface area in cm^{-2} and c is the concentration of electron in cm^{-3}. Under standard air mass conditions of 1.5, the effective diffusion depends upon light intensity of insolation and Fermi level. Electron diffusion

occurs through the TiO$_2$ framework performing external work in the conduit. The maximum power point on the I-V curve describes the magnitude of this load. The efficiency of DSC therefore depends on the reduction redox reaction at counter electrode in Eq. (1), and regeneration of oxidized dye at TiO$_2$ photoanode occurring several nanoseconds prior to recombination. The electromotive force required for these dual processes is supplied by the open circuit voltage. Past results indicated that about 50 % of original energy of photon was lost inside the solar cell but the n-Mosfet device augments the open circuit in a novel way to boost the efficiency of *T. daniellii* solar cell [20].

2. Materials and methods

2.1. Preparation of dye extract

T. daniellii dye was prepared using facile laboratory methods. 200 g of *T. daniellii* leaf was air dried until it assumed constant weight. The dried leaf was milled and spread out for 4 hours to get rid of moisture and prevent bacterial action. This dried crushed leaf sample was then soaked by immersion in 4,000 ml of methanol in TLC tanks for 11 days to extract the dye. Methanol was selected for use because records have shown that it gives better yield [7]. The resulting methanolic liquor obtained after 11 days was separated from the dye extract using sterile filters. The filtrate was feed into rotary evaporator of type Stuart RE 300 B series to recover the pure *T. daniellii* dye.

2.2. Preparation of conducting slides

Two Indium doped oxide (ITO) conducting slides of 10 ohm/m^2 surface resistivity were used on an active area of 3.16 m^2. The TiO$_2$ used for this experiment was chemically pure variety purchased from Sure Chemical Products assay 98 % min. The ZnO used had an assay of 99 %. Doctor blade method of application was used to spread on the TiO$_2$ and ZnO paste to two different batches of ITO conducting slides which were prepared using standard laboratory methods described in previous literature [9]. The effect of varying temperature (350−450 °C) in *T. daniellii* thin film was observed as air spaces were eliminated by the sintering process. The last step involved the sintering of the air dried photoanode by varying temperature from 350−450 °C to enhance good surface adsorption and eliminate air spaces. This was accomplished using Vecstar furnaces. The counter electrode was prepared by coating the TCO with soot in a vacuum-like enclosure. The result obtained was a stress-free epitaxial layer due to the differences between the lattice constant of substrate and the thin film coat. This set-up was allowed to cool before the two electrodes were fastened together with binder clips and sealed with crazy glue. Subsequently, two drops of aqueous electrolyte constituted in ratio 1 g: 100 g distilled water was introduced in-between the two electrodes to improve the mobility of charge transport. The MOSFET is connected to the common source as shown in

Fig. 1. The power Mosfet is a special type of semiconductor oxide designed to produce linear amplification by operating from its saturation region and this is enhanced by its very large value of input impedance [21].

3. Results and discussion

3.1. UV/VIS spectroscopy of *T. daniellii*

The spectrograph of *T. daniellii* shows a bathochromic shift in wavelength. It exhibits porphyrin behavior in its peak absorbance as illustrated in Fig. 2. The implication of this is that, *T. daniellii* is capable of absorbing light in two regions of the electromagnetic spectrum. It absorbs in the near ultraviolet and within the visible spectrum, this increases the allocation of solar energy available for photoexcitation.

3.2. SEM microscopy of *T. daniellii* on different photoanodes

Zeiss scanning electron microscope produces micrographs of *T. daniellii* at a width depth of 10.1 mm. Combinations of different sized cylindrical grains are arranged in a distinctive pattern of multigrain cluster amid narrow trap sites in Fig. 3(a). The
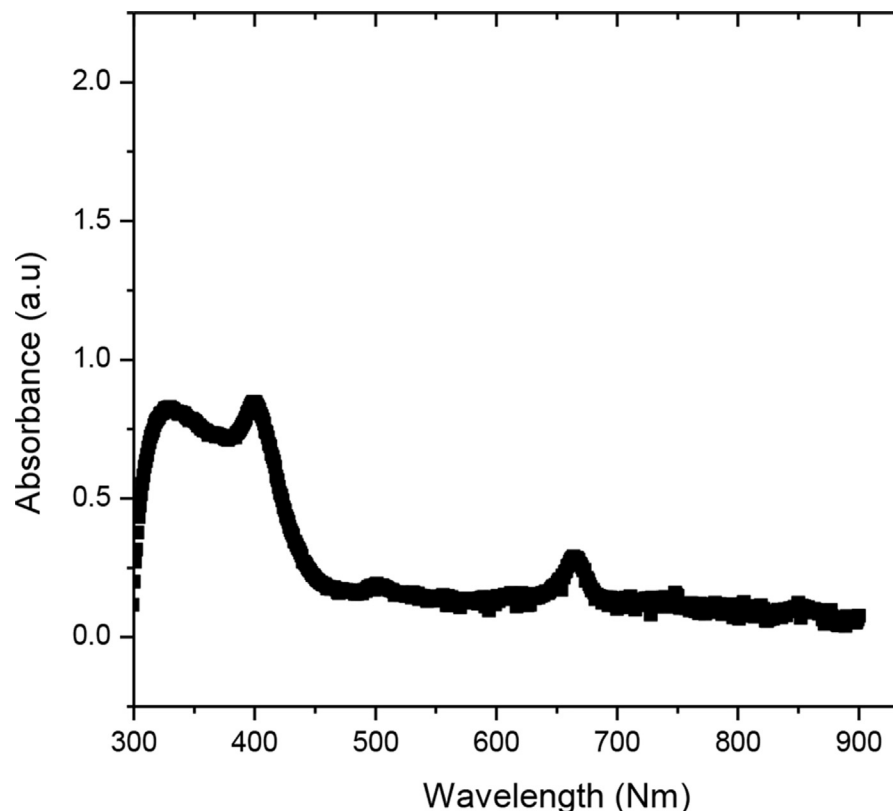

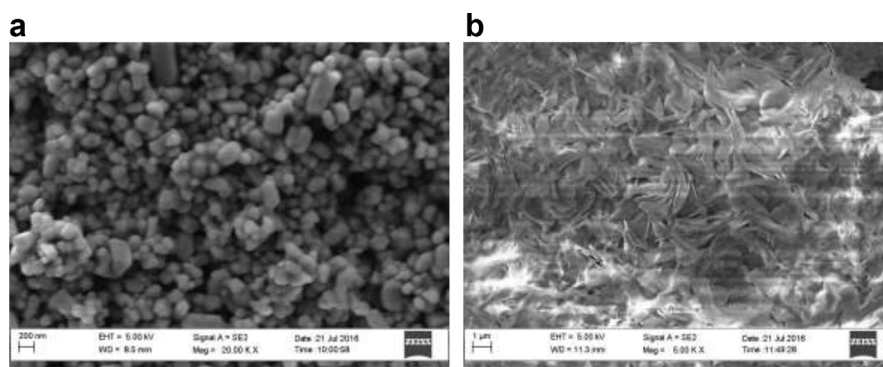**Fig. 2.** UV/VIS of *T. daniellii* leaf dye extract.

Fig. 3. The SEM micrograph of *T. daniellii* on (a) TiO$_2$ and (b) ZnO photoanode.

microstructure would enhance speedy charge transport along the boundary grain in Fig. 3(a). Recombination would possibly occur at the trap sites denoted by the dark spots. The microstructure of *T. daniellii* based on ZnO is a jelly-like mass as shown in Fig. 3(b) where charge transport by characteristic hopping would be greatly impeded by internal friction between neighboring atoms. This is collaborated by the photovoltaic results.

3.3. Effect of Z44 Mosfet on *T. daniellii* DSC doped with different ions based on different photoanodes

Gwwydion software was used to model the SEM micrograph of *T. daniellii* on TiO$_2$ and ZnO photoanodes respectively as shown in Fig. 4(a) and (b) respectively. The results are as diverse as that revealed by the SEM micrographs. The red spots depict the position of the electron and thus the energy level in *T. daniellii* dye. Thus, when exposed to light of appropriate frequency, photoexcited electrons move by series of hops to complete the conduit provided by the framework on which it rests. The blue colour represents the grain boundaries through which the electron tunnels (Nguyen et al., 2018). The kinematics of charge transport in Fig. 4(a) is more efficient because it is characterized by series of hops and diffusion due to proximity of neighboring atoms. The grain boundary is only prominent at the periphery of the framework.
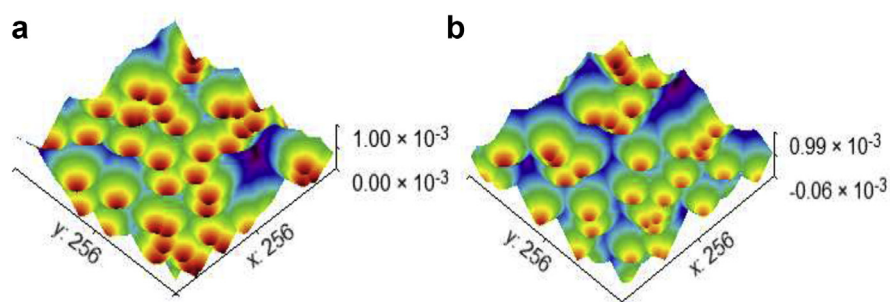

Fig. 4. Location of electron in *T. daniellii* dye extract on (a) TiO$_2$ and (b) ZnO framework.

A little tunneling completes the path of charge transport as denoted by the larger short circuit current (I_{sc}). On the other hand, Fig. 4(b) depicts more electrons enshrouded by the grain boundary, this effectively imposes a great deal of electron tunneling and possible trap sites which ultimately impedes charge transport. The I-V curve shows the impact of Z44 n-Mosfet on *T. daniellii* DSCs. It regularizes the diversity in the initial optical responses obtained from *T. daniellii* DSCs based on different photoanodes. It also acts as a stabilizer of the photovoltaic output as shown in Tables 1 and 2. This is particularly of keen scientific interest because even indirect challenges associated with DSCs, problems like the irradiance, encapsulation and other limitations become less significant in determining the output performance of *T. daniellii* DSC.

3.4. Photovoltaic results of *T. daniellii* DSC based on different photoanode

The I-V curve is a pictorial representation of charge transport and epitaxial strain on the dye membrane as the charge diffusion occurs by a series of hops across *T. daniellii* dye interface. The mobility in the MOSFET and its responsiveness as a detector can be tailored by the amount of strain and composition which defines the band gap of the thin film layer. Thus, the strain is proportional to the resistance of each thin film to charge transport. The outcome presented in Fig. 5 depicts the result of introducing different ions into the *T. daniellii* thin film framework through electrolytic

Table 1. Photovoltaic response of *T. daniellii* DSC/TiO$_2$ to doping with different ions.

Electrolyte	I_{sc} (mA)	V_{oc} (mV)	M_{pp} (W × 10^{-6})	*ff*	Efficiency (%)
HgCl$_2$	0.009	90.5	1.36	1.67	0.40
KBr	0.026	160.2	3.08	0.74	0.90
KCl	0.006	120.0	1.78	2.47	0.50
KI	0.104	240.6	12.21	0.048	0.39
Mosfet-HgCl$_2$	0.35	17.0	1.42	0.23	0.45

Table 2. Photovoltaic response of *T. daniellii* DSC/ZnO to doping with different ions.

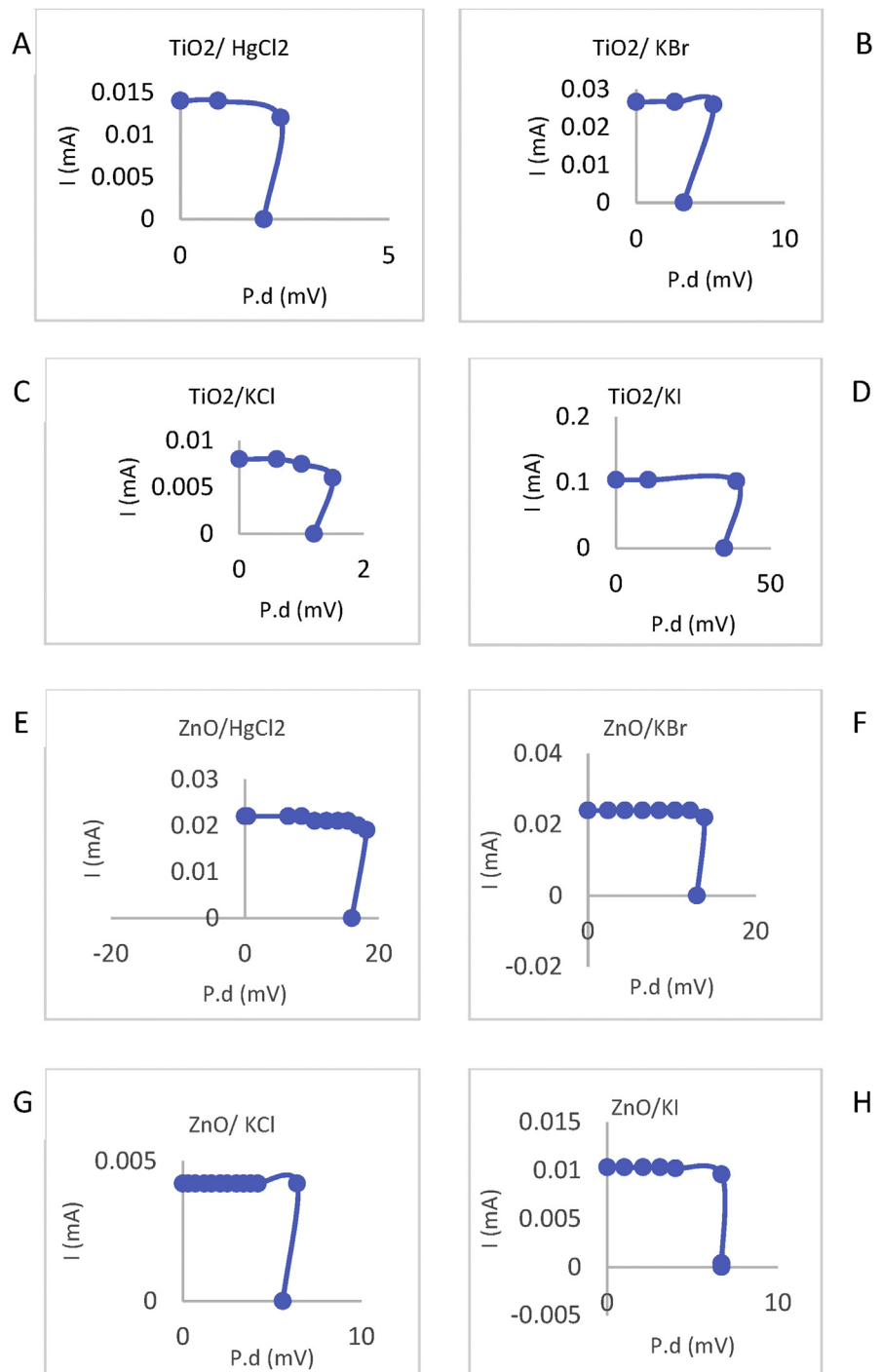| Electrolyte	I_{sc} (mA)	V_{oc} (mV)	M_{pp} (W × 10^{-6})	*ff*	Efficiency (%)
HgCl$_2$	0.05	69.0	0.669	0.19	0.002
KBr	0.0015	0.7	0.0005	0.476	1.5E-6
KCl	0.026	90.0	0.5	0.21	0.0016
KI	0.063	170.0	1.166	0.109	0.004
Mosfet-Kl	0.33	16.0	1.92	0.36	0.61

Fig. 5. (A): DSC with second highest Pmax, (B): DSC *with highest fill factor (ff)*, (C): *DSC with highest η*, (D): DSC *with least η*, (E): DSC with largest Voc, (F): DSC with largest Voc, (G): DSC with highest Isc *and* (H): DSC with highest fill factor on ZnO.
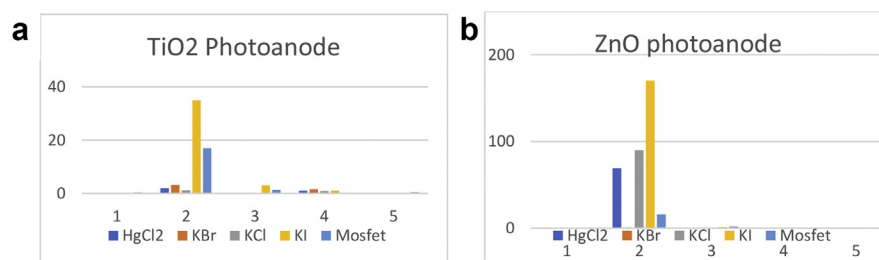
Fig. 6. Performance of n-Mosfet relative to *T. daniellii* DSCs based on (a) TiO$_2$ and (b) ZnO photoanode.

solutions, I-V curves in Fig. 5a, c, e and g are based on TiO$_2$ photoanode and the photovoltaic values for each DSC. I-V curves in Fig. 5b, d, f and h illustrate the spectral responses of *T. daniellii* DSCs based on ZnO with different electrolyte ions. Fig. 5(a) shows the effect of introducing Z44 MOSFET on the arrangement based on TiO$_2$ and (b) illustrated the same Mosfet based on ZnO. The variation in *T. daniellii* DSCs is largely due to the interboundary relationship between the dye, electrolyte and photoanode.

The roughness factor of *T. daniellii* dye is the parameter used to describe the three interface features. The result reveals that *T. daniellii* DSC based on TiO$_2$ records the highest short circuit current with KI as shown in Fig. 5(c). Thus, the best morphology is presented with l$^-$, there is an efficient use of the small photons liberated. This translates to a comparatively high V$_{oc}$ and efficiency. The initial break is from data presentation on would impede efficient charge transport as presented on Table 1. Fig. 5(b) describes a relatively large number of photons exciting *T. daniellii* dye depicted by the short circuit current value. However, the reaction kinematics is unfavourable as it progresses, this is probably as a result of iodide ions (l$^-$) ionizing with holes in the *T. daniellii* material thus creating a potential barrier creating a higher back reaction. This is equally responsible for the small value of V$_{oc}$ recorded. The roughest dye surface is also presented by *T. daniellii*/ZnO/KI as shown in Fig. 5(d) this is because of similar reasons to the TiO$_2$ photoanode. The least efficient *T. daniellii* DSC is that doped with Br$^-$. This is due to poor charge transport, unfavourable redox reactions creating a backward e.m.f shown as the low V$_{oc}$. The I-V patterns obtained owe their irregularity as depicted in Fig. 5(b), (e) and (g) to unfavorable electron dynamics and shading effect. The results illustrated in Tables 1 and 2 buttress the diversity of spectral responses obtained from *T. daniellii* dye based on dissimilar electrodes. Thus, the highlight is the n-Mosfet harmonizing these disparities despite delineating factors such as kinematics, dye morphology which normally decimates DSC photovoltaic performance. Fig. 6(a) and (b) gives a summary of photovoltaic performance from the dissimilar photoanodes. ZnO photoanode presents a better output as shown in the figures.

3.5. Conclusion and recommendations

Z44 n-Mosfet amplifies small amount of photons by a factor of approximately 50 %. Future applications in optoelectronic devices could overcome the associated problem of damped oscillations. In addition, DSC modules could incorporate the Mosfet device for improved optical spectral performance. These results recommend a technique to model novel p-i-n heterostructured DSCs which may function as photonic detectors operating in the near infrared wavelengths of $1-1.5$ μm and which may alternate as high speed MOSFETs in switching relays. Their outstanding result is that the same output voltage is accomplished for different loads. Future research would address the redox reactions and as such optimize the efficiency of other Mosfet DSCs.

Declarations

Author contribution statement

Temitope Abodunrin: Conceived and designed the experiments; Performed the experiments; Wrote the paper.

Boyo Adenike: Conceived and designed the experiments.

Mojisola Usikalu, Chester Kotsedi, Zebib Nuru, Maaza Malik: Contributed reagents, materials, analysis tools or data.

Moses Emetere, Oluseyi Ajayi, Godwin Oghonyon: Analyzed and interpreted the data.

Funding statement

Competing interest statement

The authors declare no conflict of interest.

Additional information

No additional information is available for this paper.

References

[1] J. Endres, S. Danis, G. Bauer, The misfit dislocation density profile in graded SiGe/Si (001) layers prepared at different temperatures, J. Phys. Condens. Matter 25 (17) (2013).

[2] A. Jamshidi, et al., Growth of GeSnSiC layers for photonic applications, Surf. Coatings Technol. 230 (2013) 106−110.

[3] W. Badawy, A review on solar cells from Si-single crystals to porous materials and quantum dots, J. Adv. Res. 6 (2) (2015) 123−132.

[4] E. Fortunato, P. Barquinha, R. Martins, Oxide semiconductor thin-film transistors: a review of recent advances, Adv. Mater. 24 (22) (2012) 2945−2986.

[5] H. Faber, Y.-H. Lin, S.R. Thomas, K. Zhao, N. Pliatsikas, M.A. McLachlan, A. Amassian, P.A. Patsalas, T.D. Anthopoulos, Indium oxide thin-film transistors processed at low temperature via ultrasonic spray pyrolysis, ACS Appl. Mater. Interfaces 7 (2015) 782−790.

[6] J. Park, et al., Review of recent developments in amorphous oxide semiconductor thin-film transistor devices, Thin Solid Films 520 (6) (2012) 1679−1693.

[7] J. Liu, D.B. Buchholz, R.P.H. Chang, A. Facchetti, T.J. Marks, High-performance flexible transparent thin-film transistors using a hybrid gate dielectric and an amorphous zinc indium tin oxide channel, Adv. Mater. 22 (2010) 2333−2337.

[8] P. Martyniuk, et al., New concepts in infrared photodetector designs, Appl. Phys. Rev. 1 (4) (2014).

[9] T.J. Abodunrin, A.O. Boyo, M.R. Usikalu, L. Obafemi, O. Oladapo, L. Kotsedi, Z. Yenus, M. Malik, Microstructure characterization of onion (*A. cepa*) peels and thin films for DSSCs, Mater. Res. Express 4 (3) (2017) 035503.

[10] Y.S. Rim, H. Chen, Y. Liu, S.-H. Bae, H.J. Kim, Y. Yang, Direct light pattern integration of low-temperature solution-processed all-oxide flexible electronics, ACS Nano 8 (2014) 9680−9686.

[11] R. Pillarisetty, Academic and industry research progress in germanium nanodevices, Nature 479 (7373) (2011) 324−328.

[12] H. Faber, S. Das, Y.-H. Lin, N. Pliatsikas, K. Zhao, T. Kehagias, G. Dimitrakopulos, A. Amassian, P.A. Patsalas, T.D. Anthopoulos, Heterojunction oxide thin-film transistors with unprecedented electron mobility grown from solution, Sci. Adv. 3 (3) (2017).

[13] R. Yao, Z. Zheng, Y. Zeng, X. Liu, H. Ning, S. Hu, R. Tao, J. Chen, W. Cai, M. Xu, L. Wang, L. Lan, J. Peng, All-aluminum thin film transistor fabrication at room temperature, Materials 10 (3) (2017) 222.

[14] N. Kenji, H. Ohta, A. Takagi, T. Kamiya, M. Hirano, H. Hosono, Room-temperature fabrication of transparent flexible thin-film transistors using amophous oxide semiconductors, Nature 432 (2004) 488−492.

[15] S. Assefa, F. Xia, Y. Vlasov, Reinventing germanium avalanche photodetector for nanophotonic on-chip optical interconnects, Nature 464 (7285) (2010) 80−U91.

[16] J. Meyer, S. Hamwi, M. Kröger, W. Kowalsky, T. Riedl, A. Kahn, Transition metal oxides for organic electronics: energetics, device physics and applications, Adv. Mater. 24 (2012) 5408−5427.

[17] T.J. Abodunrin, A.O. Boyo, M.R. Usikalu, C. Kotsedi, Z. Nuru, M. Malik, Performance analysis of spectral responses of *A. cepa* peel dye-sensitized solar cell to liquid electrolytes, Int. J. Civ. Eng. Technol. 9 (8) (2018).

[18] S. Wirths, et al., Lasing in direct-bandgap GeSn alloy grown on Si, Nat. Photon. 9 (2) (2015) 88−92.

[19] K. Nomura, H. Ohta, K. Ueda, T. Kamiya, M. Hirano, H. Hosono, Thin-film transistor fabricated in single-crystalline transparent oxide semiconductor, Science 300 (2003) 1269−1272.

[20] Y.H. Hwang, J.-S. Seo, J.M. Yun, H. Park, S. Yang, S.-H.K. Park, B.-S. Bae, An 'aqueous route' for the fabrication of low-temperature-processable oxide flexible transparent thin-film transistors on plastic substrates, NPG Asia Mater. 5 (45) (2013). https://www.nature.com/articles/am201311.

[21] J.H. Park, F.H. Alshammari, Z. Wang, H.N. Alshareef, Interface engineering for precise threshold voltage control in multilayer-channel thin film transistors, Adv. Mater. Interfaces (2016) 1600713.